



## Original Article

## Targeted delivery of Chinese herb pair-based berberine/tannin acid self-assemblies for the treatment of ulcerative colitis



Shiyun Chen<sup>a,1</sup>, Zhejie Chen<sup>a,1</sup>, Yi Wang<sup>b</sup>, Wei Hao<sup>a</sup>, Qin Yuan<sup>a</sup>, Hefeng Zhou<sup>c</sup>, Caifang Gao<sup>a</sup>, Yitao Wang<sup>a</sup>, Xu Wu<sup>b,\*</sup>, Shengpeng Wang<sup>a,\*</sup>

<sup>a</sup>State Key Laboratory of Quality Research in Chinese Medicine, Institute of Chinese Medical Sciences, University of Macau, Macao

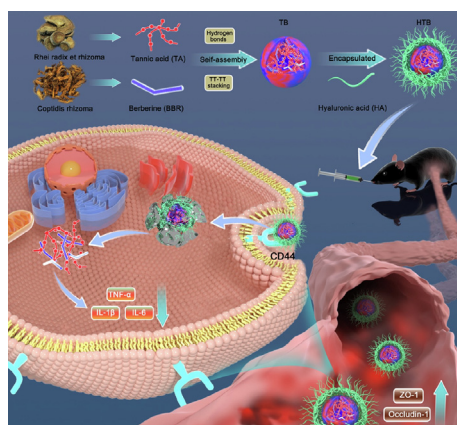
<sup>b</sup>Laboratory of Molecular Pharmacology, Department of Pharmacology, School of Pharmacy, Southwest Medical University, Luzhou, Sichuan, China

<sup>c</sup>Department of Bioengineering, Zuhai Campus of Zunyi Medical University, Zuhai, China

## HIGHLIGHTS

- A colon-targeted hyaluronic acid-coated berberine/tannin acid nanostructure (HTB) was developed
- HTB could localize in inflamed colon in colitis mice
- HTB exerted strong therapeutic efficacy in mouse model of colitis
- HTB regulated gut barrier function and apoptosis in colitis mice
- HTB partially recovered DSS-mediated gut microbiome alteration

## GRAPHICAL ABSTRACT



## ARTICLE INFO

## Article history:

Received 26 September 2021

Accepted 24 November 2021

Available online 29 November 2021

## ABSTRACT

**Introduction:** Ulcerative colitis (UC) is a chronic recurrent idiopathic disease characterized by damage to the colonic epithelial barrier and disruption of inflammatory homeostasis. At present, there is no curative therapy for UC, and the development of effective and low-cost therapies is strongly advocated.

**Abbreviations:** ANOVA, Analysis of variance; BBR, Berberine; BrdU, Bromodeoxyuridine; BSA, Bovine serum albumin; CD44, Cluster of differentiation 44; CLSM, Confocal laser scanning microscopy; CM, Chinese medicine; CTAB, Cetyltrimethylammonium bromide; Cy3, Cyanine-3; DAB, 3,3'-Diaminobenzidine; DAI, Disease activity index; DAPI, 4'-6-Diamidino-2-phenylindole; DLS, Dynamic light scattering; DMEM, Dulbecco's Modified Eagle Medium; DP, Differential power; DSS, Dextran sodium sulfate; EDTA, Ethylenediaminetetraacetic acid; EE, Encapsulation efficiency; ELISA, Enzyme-linked immunosorbent assay; FCM, Flow cytometry; FITC, Fluorescein isothiocyanate; FLASH, Fast Length Adjustment of SHort reads; FTIR, Fourier-transform infrared spectroscopy; HA, Hyaluronic acid; HRP, Horseradish peroxidase; IHC, Immunohistochemistry; ITC, Isothermal titration calorimetry; KA, Equilibrium association constant; KD, Equilibrium dissociation constant; LDA, Linear discriminant analysis; LE, Loading efficiency; MDA, Malondialdehyde; MPO, Myeloperoxidase; MW, Molecular weight; NCM460, Normal human colon mucosal epithelial cell; NIR dye, Near infrared dye; OTU, Operational taxonomic unit; PBS, Phosphate-buffered saline; PCR, Polymerase chain reaction; PDI, Polydispersity index; RDP, Ribosomal database project; R123, Rhodamine 123; ROI, Region of interest; RPMI1640 Medium, Roswell Park Memorial Institute 1640 Medium; SDS, Sodium dodecyl sulfate; TA, Tannic acid; TEM, Transmission electron microscopy; UC, Ulcerative colitis; UV-vis, Ultraviolet-visible; XRD, X-ray diffraction; ZO-1, Zonula occludens-1;  $\Delta H$ , Enthalpy;  $\Delta S$ , Entropy; 5-ASA, 5-Aminosalicylic acid.

Peer review under responsibility of Cairo University.

\* Corresponding authors at: University of Macau, Avenida da Universidade, Taipa 999078, Macao (S. Wang).

E-mail addresses: [wuxulz@126.com](mailto:wuxulz@126.com) (X. Wu), [swang@um.edu.mo](mailto:swang@um.edu.mo) (S. Wang).

<sup>1</sup> These authors contributed equally to this work.

<https://doi.org/10.1016/j.jare.2021.11.017>

2090-1232/© 2022 The Authors. Published by Elsevier B.V. on behalf of Cairo University.

This is an open access article under the CC BY-NC-ND license (<http://creativecommons.org/licenses/by-nc-nd/4.0/>).

**Keywords:**

Berberine  
Tannin acid  
Ulcerative colitis  
Drug delivery  
Gut microbiome

**Objectives:** Multiple lines of evidence support that tannic acid (TA) and berberine (BBR), two active ingredients derived from Chinese herb pair (Rhei Radix et Rhizoma and Coptidis Rhizoma), have promising therapeutic effects on colonic inflammation. This study aims to develop a targeted delivery system based on BBR/TA-based self-assemblies for the treatment of UC.

**Methods:** TA and BBR self-assemblies were optimized, and hyaluronic acid (HA) was coated to achieve targeted colon delivery via HA-cluster of differentiation 44 (CD44) interactions. The system was systematically characterized and dextran sodium sulfate (DSS)-induced mouse colitis model was further used to investigate the biodistribution behavior, effect and mechanism of the natural system.

**Results:** TA and BBR could self-assemble into stable particles (TB) and HA-coated TB (HTB) further increased cellular uptake and accumulation in inflamed colon lesions. Treatment of HTB inhibited pro-inflammatory cytokine levels, restored expression of tight junction-associated proteins and recovered gut microbiome alteration, thereby exerting anti-inflammatory effects against DSS-induced acute colitis.

**Conclusion:** Our targeted strategy may provide a convenient and powerful platform for UC and reveal new modes of application of herbal combinations.

© 2022 The Authors. Published by Elsevier B.V. on behalf of Cairo University. This is an open access article under the CC BY-NC-ND license (<http://creativecommons.org/licenses/by-nc-nd/4.0/>).

## Introduction

Ulcerative colitis (UC) is a multifactorial disorder of the intestinal tract that induced by chronic inflammation [1]. In the past decade, the incidence of UC has experienced a more than doubled increase in several countries [2]. With no curative therapy for UC at present, it is often necessary to take medication in a long-term and standardized manner to relieve and reduce the recurrence rate [3]. It is estimated that the lifetime cost of UC is equivalent to the cost of major diseases such as cardiovascular diseases and cancer, which seriously affect the patients' quality of life. Thus, the development of effective and low-cost therapeutics is of significance and necessary for the patients with UC. Recently, a spectrum of studies have indicated the efficacy of the natural compounds isolated from Chinese medicine (CM) in the treatment of UC. These bioactives could potentially inhibit intestinal inflammation and enhance the wound healing via manifold mechanisms [4]. Although the application of many CM or the derived active constituents has achieved promising therapeutic potentials in experimental UC models, the wide use of CM is largely limited due to poor solubility, instability, short half-life, and low selectivity [5].

Combination of multiple herbs is one of the most important characteristics of CM [6,7]. Interestingly, recent studies have shown some modes of interactions among active constituents of herbs. For instance, Coptidis Rhizome (the rhizome of *Coptis chinensis* Franch., *C. deltoidea* C.Y. Cheng et Hsiao, or *C. teeta* Wall) [8,9] and Scutellariae Radix (the root of *Scutellaria baicalensis* Georgi.) [10] are traditionally used as a representative herb pair for treatment of gastrointestinal tract disorders. Berberine (BBR) from Coptidis Rhizoma and baicalin, a bioactive flavone glucoside derived from Scutellariae Radix, could assemble in water into nanostructures, which showed superior bacteriostatic activity [11]. Similar synergistic self-assemblies were also found between BBR and cinnamic acid, a monocarboxylic acid found in Cinnamomi Cortex (the dried bark of *Cinnamomum verum*), which were derived from another herb pair (Coptidis Rhizoma and Cinnamomi Cortex) [12].

Inspired by the traditional combination of Rhei Radix et Rhizoma (the dried roots and rhizomes of *Rhym palmatum* L, *Rheum tanguticum* Maxim. ex Balf., or *Rhum officinal* Bail. in Polygonaceae family) and Coptidis rhizoma in clinic [13,14], a promising way was proposed here to have favorable therapeutic effects upon inflammatory states in colon based on the self-construction of natural constituents. Several lines of evidence have supported the notion that BBR (Fig. 1A), a major alkaloid of Coptidis Rhizoma, has a longstanding use in China and a favorable therapeutic effect

upon inflammatory states in the colon as demonstrated across of variety of models and clinical trials [15,16]. Tannic acid (TA, Fig. 1A) is a natural polyphenol that can be found in red wine, black tea, green tea and many herbal medicines like Rhei Radix et Rhizoma, which possesses protective benefits in conditions of acute or chronic intestinal inflammation [17]. Our present study found that TA and BBR could self-assemble into uniform and stable particles (TB) in aqueous solution, which might be attributed to the formation of hydrogen bonds and  $\pi$ - $\pi$  stacking interactions of the two compounds. Moreover, the expression of cluster of differentiation 44 (CD44) was reported to be increased on the surface of colonic epithelial cells and macrophages in colitis tissue [18], we further propose to target CD44 by superimposing negatively HA on the surface of positively charged TB and prepare a novel targeted delivery system (HTB) via HA-CD44 interaction for inflammatory colonic epithelial cells and pro-inflammatory macrophages through HA-CD44 interaction. The system was systematically characterized, and dextran sodium sulfate (DSS)-induced colitis mouse model was further used to investigate the biodistribution behavior, effect and mechanism of the natural system against UC. Our targeted strategy may provide a convenient yet powerful platform for UC and reveal new modes of application of herbal combinations.

## Materials and methods

### Materials

BBR and TA were purchased from Shanghai Yuanye Biological Technology Co., Ltd. (Shanghai, China) and Sigma-Aldrich Company (St. Louis, MO, USA), respectively. HA was purchased from Lifecore Biomedical, LLC (Minnesota, USA). IR780 was obtained from J & K Technology Co., Ltd. (Shanghai, China). Rhodamine 123 (R123) was supplied by Shanghai Macklin Biochemical Co., Ltd. (Shanghai, China). 5-Aminosalicylic acid (5-ASA) was purchased from Merck & Co Inc (New Jersey, USA). DSS (Mw 36–50 kDa) was obtained from MP Biomedicals LLC (California, USA). Enzyme-linked immunosorbent assay (ELISA) kits including interleukin-1 $\beta$  (IL-1 $\beta$ ) kit, Tumor necrosis factor-alpha (TNF- $\alpha$ ) kit and IL-6 kit were supplied from Biolegend (California, USA). Myeloperoxidase (MPO) and malondialdehyde (MDA) kits were purchased from Nanjing Jiancheng Biological Engineering Research Institute (Nanjing, China). Hydrogen peroxide (H<sub>2</sub>O<sub>2</sub>) kit was obtained from Beijing Solarbio Science & Technology Co., Ltd. (Beijing, China). Bovine serum albumin (BSA) was supplied from BioFroxx (Germany). Rabbit anti-occludin antibody (Bs-10011R) and rabbit anti-Bromodeoxyuridine (BrdU, pro-

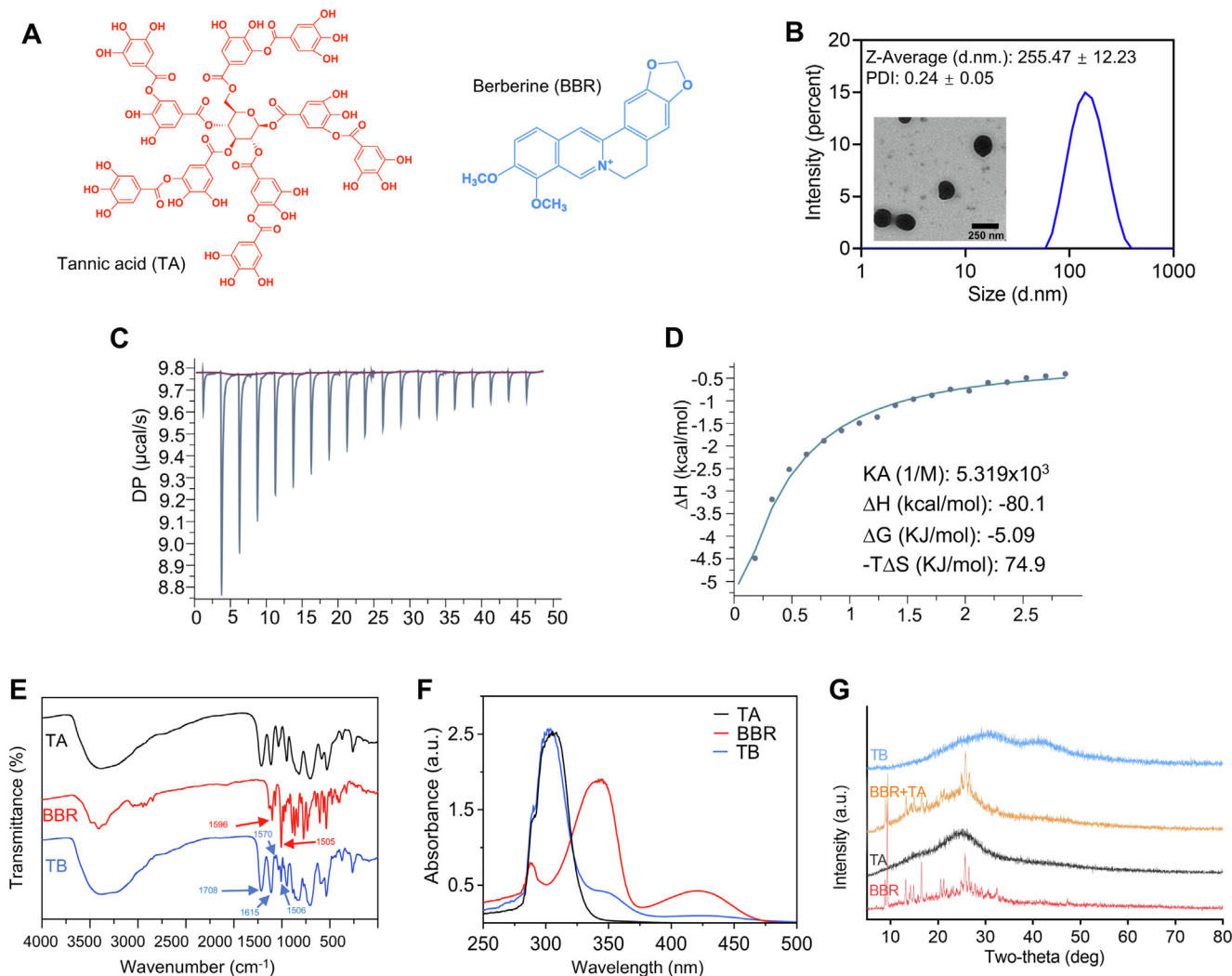


**Fig. 1.** Preparation and characterization of TB. (A) Chemical structures of TA and TB. (B) Size distribution and morphology of TB. Data are expressed as mean  $\pm$  SD ( $n = 3$ ). (C) ITC raw data of TB. (D) Fitted curves and thermodynamic parameters of the titration of TB. (E) Infrared radiation profiles of TB and their monomers. (F) UV-Vis spectroscopy of TB and their monomers. (G) XRD profiles of TB and their monomers.

liferation marker) antibody were purchased from Bioss (Beijing, China). Zonula Occludens-1 (ZO-1) and beta Catenin monoclonal antibodies were obtained from Affinity (Xiamen, China). Fluorescein isothiocyanate (FITC) conjugated goat anti-rabbit IgG (H + L), cyanine-3 (Cy3) conjugated goat anti-rabbit IgG (H + L), and horseradish peroxidase (HRP)-labeled goat anti-rabbit IgG were all supplied from Servicebio Technology Co. Ltd. (Wuhan, China). Ethylenediaminetetraacetic acid (EDTA) antigen repair solution, citric acid (pH 6.0), antigen repair solution, hematoxylin staining solution, autofluorescence quencher and 4'-6-diamidino-2-phenylindole (DAPI) were all purchased from Beijing Solarbio Science & Technology Co. Ltd (Beijing, China).

#### Ethics statement

All experiments involving animals were conducted according to the ethical policies and procedures approved by the committee on Use and Care of Animals of University of Macau, Macau (Ethics No.: UM ARE-037-2018). Male C57BL/6 mice (22–25 g) were obtained from Faculty of Healthy Science Animal Centre of University of Macau. Experimental animals were housed under standard feeding environment of mice and supplied ad libitum with feed and pure water.

#### Preparation of HTB

BBR and TA were completely dissolved in deionized water and prepared into different concentrations of BBR and TA stock solutions at 25 °C, respectively. BBR aqueous solution was slowly dropped into TA aqueous solution at different molar ratios (BBR: TA at 1: 3, 1: 2, 1: 1, 2: 1 and 3: 1). After being stirred and heated for 30 min, the self-assembly solution was put into a dialysis bag ( $M_w$  2 kDa) to dialyze against ultra-pure water for 12 h. The Tindal effect was observed in the self-assembly solution. To coat TB with HA, the self-assembly solution was slowly added to the HA aqueous solution (1 mg/mL), which was further stirred at 25 °C for 15 min to obtain the HTB solution. The HTB particle solution was stored at 4 °C or lyophilized with a freeze dryer for further use [19].

#### Physicochemical characterization of HTB

The particle sizes, zeta-potentials and polydispersity index (PDI) of TB and HTB were determined by dynamic light scattering (DLS) which was equipped with a Malvern Zetasizer Nano ZS system (Malvern Instruments, Malvern, UK) at 25 °C.

Images of morphology and size of self-assembled structures were scanned via transmission electron microscopy (TEM, JEM

1200X, JEOL, Japan). A small amount of aqueous solution of TB or HTB was placed on a carbon-coated copper grid, then the excess solution was dried after 5 min. Next, uranyl acetate was employed to stain TB or HTB sample, and then TEM analysis was put into practice.

The spectroscopy properties of TA, BBR and TB were analyzed by Fourier transform infrared spectroscopy (FT-IR) at the range of 4000–500  $\text{cm}^{-1}$  via the KBr method. The ultraviolet–visible (UV–Vis) absorption spectras were acquired by using a UV–Vis spectrophotometer (HACH DR6000, Japan) in the scanning range of 250–500 nm.

The X-ray diffraction (XRD) spectra of TA, BBR, the physical mixture of TA and BBR and TB were detected by X-ray diffractometer (D8 Advance, BRUKER, Germany). The detection condition was set to scan and record at the speed of 8°/min under 40 kV and 40 mA from 5° to 80°.

The loading efficiency (LE) and encapsulation efficiency (EE) of BBR were measured using the UV–Vis spectrophotometer at 421 nm. The TB and HTB suspensions containing BBR were centrifuged by ultrafiltration centrifuge tube ( $M_w$  10 kDa) at 4500 rpm for 30 min at 4 °C. The amount of free BBR in the supernatant was calculated according to BBR standard solutions. The EE and LE of BBR were calculated as follows [19]:

$$EE (\%) = [(total\ BBR - free\ BBR) / total\ BBR] \times 100\%$$

$$LE (\%) = [(total\ BBR - free\ BBR) / total\ quality] \times 100\%$$

#### Formation mechanism test by isothermal titration calorimetry (ITC)

ITC assay was performed on a MICROCAL PEAQ-ITC (Malvern, UK) [20]. The BBR aqueous solution (1.8 mM) was injected into a 0.12 mM TA aqueous solution at a 2-min interval to achieve complete equilibration of the solution system between each two injections. 2.5  $\mu\text{L}$  TA aqueous solution was injected into the sample cell for 20 times. All ITC assays were performed at 25 °C. The injection of BBR aqueous solution (1.8 mM) into deionized water was employed as the benchmark. After the deduction of the dilution heat of TA aqueous solution, the obtained data were fitted to a theoretical titration curve.

#### Stability of HTB

The stability experiment of TB and HTB were performed in a storage period of up to 15 days. For the 15-day stability study, the size distribution, zeta-potential and PDI of TB and HTB were observed via DLS on day 1, 3, 7, 10 and 15, respectively.

#### Cell culture

Raw264.7 and NCM460 colon mucosal epithelial cell lines were purchased from the American Type Culture Collection (Manassas, VA, US). Raw264.7 cells were cultured in Dulbecco's Modified Eagle Medium (DMEM) (Gibco) added extra 10% fetal bovine serum (FBS, Thermo Fisher Scientific, Billerica, USA). NCM460 cells were cultured in Roswell Park Memorial Institute 1640 (RPMI 1640) Medium (Gibco) contained with 10% FBS and 1% penicillin and streptomycin. Both cell lines were cultured in a humidified 5%  $\text{CO}_2$  atmosphere at 37 °C.

#### Evaluation of cellular uptake

In order to qualitative analysis the differences of cellular uptake characteristics, Raw264.7 and NCM460 cells were separately seeded into confocal dishes and cultured overnight. Fluorescent probe R123 was effectively encapsulated into TB and HTB for cellular

uptake assay. Unbound R123 was separated from the R123-containing self-assemblies through high-speed centrifugation. To further investigate the active targeting mechanism of HTB, both cell lines were incubated with 1 mg/mL of HA for 4 h before treatment with HTB. Then, HTB and TB at the same fluorescence concentration (0.42  $\mu\text{g}/\text{mL}$  R123) were added and incubated respectively for 4 h at 37 °C. Untreated cells were employed as a control group in the experiment. Cells were then stained with Hoechst 33,342 for 30 min, washed twice using phosphate-buffered saline (PBS), and fixed in 4% paraformaldehyde stationary solution for 10 min for further imaging analysis by using a confocal laser scanning microscopy (CLSM, LEICA TC8 SP8, Germany).

Flow cytometer (BD LSRFortessa, USA) was utilized to quantitatively analyze the cellular uptake of HTB and TB. Briefly, Raw264.7 and NCM460 cells were seeded into 12-well plates and treated as aforementioned, then the cells were washed for three times with PBS and made into the single-cell suspension. The fluorescence intensity was determined by the flow cytometry (FCM).

#### Evaluation of adhesion effect of HTB

A DSS-induced experimental UC model was established in C57BL/6 mice. Near infrared dye (NIR dye) IR780 (maximum absorbance 780 nm) was loaded in HTB and TB (IR780-HTB and IR780-TB) as previously reported [21]. NIR fluorescence images were scanned by an *in vivo* image formation system (IVIS Lumina XR III, USA). Briefly, experimental mice were randomly divided into 3 groups ( $n = 6$ ), namely water + IR780-HTB group, DSS + IR780-TB group and DSS + IR780-HTB group. Water + IR780-HTB group was administered with normal distilled water as a control group, and DSS + IR780-TB group and DSS + IR780-HTB group were given with DSS solution (3%, w/v) for 7 days to establish experimental UC model. Then mice were scanned via a living imaging system after intragastric administration at four consecutive time points (3, 6, 12, and 24 h). After the live imaging shooting of the final time point, mice were sacrificed immediately, and the colons was completely separated by dissection and detected for fluorescence without any cleaning process.

#### *In vivo* therapeutic evaluation

The therapeutic effect of HTB was evaluated in DSS-induced C57BL/6 colitis model [22]. Briefly, experimental animals were divided into five groups ( $n = 6$ ) at random as follows: control group, model group, 5-ASA group, TB group, and HTB group. Mice in model, 5-ASA, TB and HTB groups were given free access to drinking water containing DSS (3%, w/v) for 6 consecutive days to establish UC model. The 5-ASA, TB and HTB groups were orally gavaged with 5-ASA (100 mg/kg), TB (containing 20 mg/kg BBR), and HTB (containing 20 mg/kg BBR) at day 3, 5, 7 and 9 (4 times in total). Model group mice received normal saline accordingly. The control group was given normal drinking water, and orally treated equivalent normal saline. Body weight of mice was recorded daily. Disease activity index (DAI) was assessed throughout the experiment according to the summation of fecal bleeding (0–4), body weight loss (0–4), and stool consistency (0–4) (Table S1) [23]. After 11 days, mice were anesthetized with pentobarbital sodium solution, and mouse blood was collected by eyeball extraction. After standing at room temperature for 30 min, the blood was centrifuged at 3000 rpm for 5 min to acquire serum. Fecal specimens from mice were collected at the day before sacrifice for gut microbial analysis. The colon tissues were harvested. Serum  $\text{H}_2\text{O}_2$ , MDA and MPO levels were tested using commercial kits according to the manufacturers' instructions. The level of pro-inflammatory cytokines in colon tissue, including IL-6, IL-1 $\beta$  and TNF- $\alpha$ , were detected via corresponding ELISA kits. Colons

were fixed in 4% paraformaldehyde stationary solution. After dehydration, colon tissues were completely embedded in paraffin and sectioned into 5- $\mu$ m slices, followed by H&E staining.

#### *In vivo immunohistochemistry imaging*

To determine the expression level of occludin and ZO-1 in colon tissue of each group, immunohistochemistry (IHC) experiment was employed. The paraffin-embedded tissue sections were dewaxed, followed by antigen repair via placing dewaxing tissue in citric acid antigen repair buffer. Then the endogenous peroxidase was blocked by incubating with 3% hydrogen peroxide solution. After blocking with 3% BSA solution, tissue sections were sequentially incubated with rabbit anti-occludin antibody (catalog#Bs-10011R) and ZO-1 antibody (catalog#AF5145) and HRP-labeled goat anti-rabbit IgG (catalog#GB23303), then stained with hematoxylin and 3,3'-Diaminobenzidine (DAB) and scanned under the Nikon Eclipse Ts2R-FL microscope system.

#### *In vivo immunofluorescence imaging*

The apoptosis and proliferation of colonic epithelium were examined by immunofluorescence. The mouse colon tissue was fixed for by xylene and washed by alcohol, then the fixed colon tissue was placed in the repair buffer containing EDTA (pH = 8.0). After incubation with BSA for 30 min, anti-mouse beta catenin monoclonal antibody (catalog#BF8016) and rabbit anti-BrdU antibody (catalog#BS-0489R) were added to the slide overnight. After washing the slides were incubated by FITC conjugated goat anti-rabbit IgG (H + L) (catalog#GB22403) and cy3 conjugated goat anti-rabbit IgG (H + L) (catalog#GB21303) for 50 min and then washed for 3 times. The cell nucleus was labeled by DAPI. Then the slides were examined by immunofluorescence microscope (Nikon Eclipse C1, Nikon, Japan).

#### *Gut microbial analysis*

Fecal DNA of mice in each group was extracted through cetyltrimethylammonium bromide/sodium dodecyl sulfate (CTAB/SDS) method. 16S (V3-V4) rRNA genes were amplified using specific primers (341F-806R). The polymerase chain reaction (PCR) products were purified by using the AxyPrepDNA Gel Extraction Kit (AXYGEN). Sequencing of 16S rRNA genes was carried out on Illumina Miseq/HiSeq2500 platform on the basis of the standard protocol of Shanghai Applied Protein Technology (Shanghai, China), and 250 bp/300 bp paired-end reads were produced and further merged utilizing Fast Length Adjustment of SHort reads (FLASH) [24]. Sequences analysis was performed with UPARSE software through the UPARSE-OTUref and UPARSE-OTU algorithms. Sequences with over 97% similarity were assigned to the same operational taxonomic unit (OTU). The ribosomal database project (RDP) classifier was employed to annotate taxonomic information for each typical sequence. The  $\alpha$  diversity (Observed species, Chao1 and Shannon),  $\beta$  diversity via principal co-ordinates analysis (PCoA) at OTU level, taxonomy analysis, and quantitative analysis of biomarkers within different groups via linear discriminant analysis (LDA) effect size (LEfSe) were conducted according to the online MicrobiomeAnalyst (<https://www.microbiomeanalyst.ca/>) [25].

#### *Statistical analysis*

All experiment results are shown as mean  $\pm$  standard deviation (SD). All assay data were corroborated in at least 3 independent tests under the unchangeable conditions. The computational part of statistics were carried out via a unpaired Student's *t*-test or

one-way analysis of variance (ANOVA) with Tukey test [26]. Statistical significance was indicated as \**P* < 0.05, \*\**P* < 0.01 and \*\*\**P* < 0.001.

## **Results and discussion**

### *Preparation of TB*

As mentioned above, the prerequisite for preparation of HTB requires the self-assembly of TA and BBR to form TB. As shown in Table S2, the proportion screening of TA and BBR showed that the average size of TB ranged from 208 to 420 nm and the zeta potential of TB ranged from 36.7 to 53.3 mV with the variation of BBR/TA substance ratio. By comprehensively analyzing the particle size, zeta potential, EE and LE, the molar ratio of BBR/TA was optimized as 2: 1 (BBR, 0.5 mg/mL; TA, 1.25 mg/mL) for preparation of TB. When the ratio of BBR to TA was 2: 1, TB with size of 255.47  $\pm$  12.23 nm and zeta potential of 46.70  $\pm$  0.72 mV showed high EE (73.03  $\pm$  3.83%) and LE (26.38  $\pm$  1.22%). TEM image also showed that the TB self-assemblies formed by TA and BBR had a uniform spherical structure which was well defined and structurally sound (Fig. 1B).

### *Formation mechanism of TB*

To further investigate the thermodynamic mechanism of interaction between BBR and TA, ITC was applied for examining the thermodynamic parameters in a TA-BBR solution. ITC works by directly measuring the heat that is either released or absorbed during a biomolecular binding event and then uses the MicroCal PEAQ-ITC analysis software to accurately determine the equilibrium dissociation constant (KD), enthalpy ( $\Delta$ H), and entropy ( $\Delta$ S). The enthalpy ( $\Delta$ H) was derived directly from the isotherm. And the nonlinear fitting algorithm was used to fit the isotherm to a site binding model from which the affinity (KD) is derived.

Thermodynamic parameters of the interactions between TA and BBR are shown in Fig. 1D. The low negative Gibbs energy change values ( $\Delta$ G) suggested that interaction of TA and BBR occurred spontaneously. The negative value of enthalpy ( $\Delta$ H) supported that the binding of BBR with TA was an enthalpy-driven reaction, which could be interpreted as molecules with opposite charges in TA-BBR interaction [27]. Furthermore, the negative  $T\Delta$ S indicated that the hydrophobic interaction of TA-BBR may also reduce energy homogeneity [11]. The downward energy change curve in Fig. 1C showed the exothermic process during the titration of TA by BBR. Therefore, the results of ITC experiment provided the thermodynamic evidence that the formation of TA-BBR assembly was a spontaneous process.

### *Characterization of TB*

The FT-IR spectra were analyzed for the binding sites of the two-component self-assembly. The results showed that the peak at 3450  $\text{cm}^{-1}$  was generated by the stretching vibration of the hydroxyl group. The peak at 1708  $\text{cm}^{-1}$  corresponded to the carboxyl carbonyl group and the peak at 1615  $\text{cm}^{-1}$  indicated the presence of C=C in the aromatic ring [28]. The characteristic band of berberine at 1505  $\text{cm}^{-1}$  (C=C stretching vibration in the aromatic ring) was observed from the spectrum of the TB. Moreover, a new small peak at 1570  $\text{cm}^{-1}$  could be observed for the TA-BBR self-assembly, which was consistent with the corresponding C=N stretching vibration at 1596  $\text{cm}^{-1}$  on BBR [29]. After the self-assembly with BBR, this peak shifted to a lower wave number, which might be due to electrostatic interactions that not only led to weaker bond strengths but also slowing down the frequency

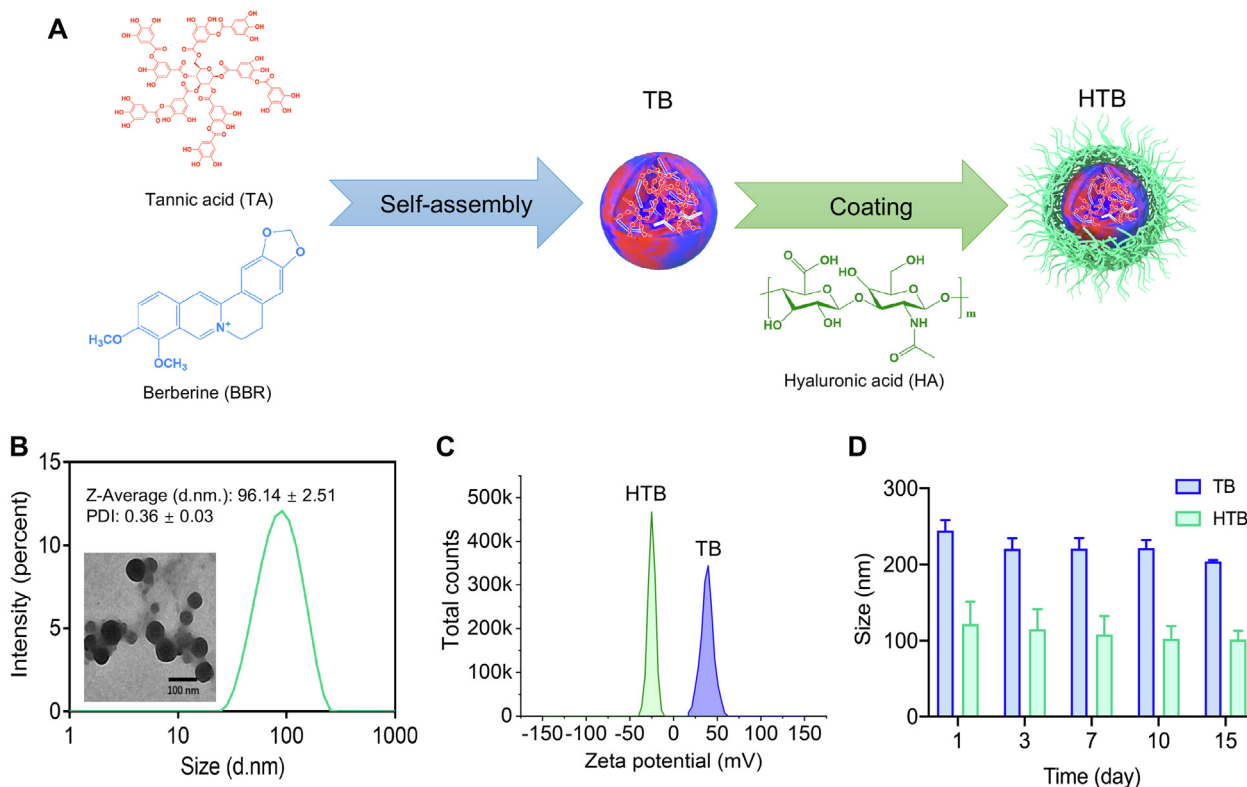


**Fig. 2.** Preparation and characterization of HTB. (A) Schematic diagram of preparing HTB. (B) Size distribution and morphology of HTB. (C) Zeta-potential distribution of HTB and TB. (D) Stability of size distribution of TB and HTB. Data are expressed as mean  $\pm$  SD ( $n = 3$ ).

of the C=N double bond stretching vibration. These results confirmed that the formation of TB from TA and BBR (Fig. 1E). To explore the structural features of TB, UV-Vis absorption spectrum was also captured. The characteristic absorption peaks of TA and BBR appeared at 310 nm and 345 nm, while the maximum absorption of TB was at 305 nm, indicating that the simultaneous existence of TA and BBR in TB self-assemblies was obtained (Fig. 1F). As revealed in Fig. 1G, the typical XRD diffractogram of BBR, TA and physical mixture of BBR and TA showed massive sharp peaks, suggesting that they had crystalline properties. In contrast, TB powders did not have these typical peaks, demonstrating no crystalline complex produced. These results provided evidence that BBR was effectively encapsulated in TB.

#### Preparation and characterization of HTB

As shown in Fig. 2A, HTB was obtained by slow titration of TB solution into HA solution (BBR, at 0.5 mg/mL, TA at 1.25 mg/mL and HA at 1 mg/mL). To characterize the HTB particles, the size of the particles and the microscopic morphology were determined by DLS and TEM, respectively. Results showed that coating with HA reduced the size distribution of the TB particles, which was changed from  $255.47 \pm 12.23$  nm to  $96.14 \pm 2.51$  nm (Fig. 2B). The change in particle size might be caused by the further compression of particles after the addition of HA. Interestingly, coating with HA reversed the zeta-potential of TB from positive to negative ( $-26.97 \pm 0.83$  mV) (Fig. 2C), which might be attributed to the negative potential of HA. Moreover, the HTB also showed a high EE ( $73.64 \pm 1.46\%$ ) and LE ( $21.69\% \pm 0.99\%$ ). Taken together, these results indicated that HA can effectively coat on TB and form evenly distributed particles.

#### Evaluation of stability

The size and zeta-potential of TB and HTB were recorded on day 1, 3, 7, 10, and 15, respectively, and the results are shown in Fig. 2D and Fig. S1. The particle size of TB and HTB did not show obvious change and the surface potential of TB and HTB was maintained at about 40 mV and  $-30$  mV for 15 days, respectively. Similarly, the size and surface potential of HTB were also Therefore, it was concluded that both TB and HTB exhibited good stability performance.

#### Cellular uptake of HTB

After incubation with R123-labeled TB or HTB for 4 h, the cellular fluorescence intensity were determined by CLSM and FCM. As shown in Fig. 3 A & B, a stronger fluorescence was observed in HTB-treated Raw264.7 and NCM460 cells as compared with that of the TB group. Similar results were also observed in quantitative analysis using FCM (Fig. 3 C & D). However, after pretreatment with HA, the intensity of intracellular fluorescence in both Raw264.7 and NCM460 cells was lower in comparison with the group treated with HTB alone (Fig. 3). These results indicated that HA may promote the cellular uptake of HTB particles through HA-CD44 interaction.

#### HTB accumulates in inflamed colon

Effectively targeting of inflammatory colonic ulcer lesions is the key factor for successful drug intervention of UC [30]. The increased expression of positively charged proteins, such as transferrin [31], bactericidal/permeability-increasing protein [32] and antimicrobial peptides [33], is one of the major characteristics of

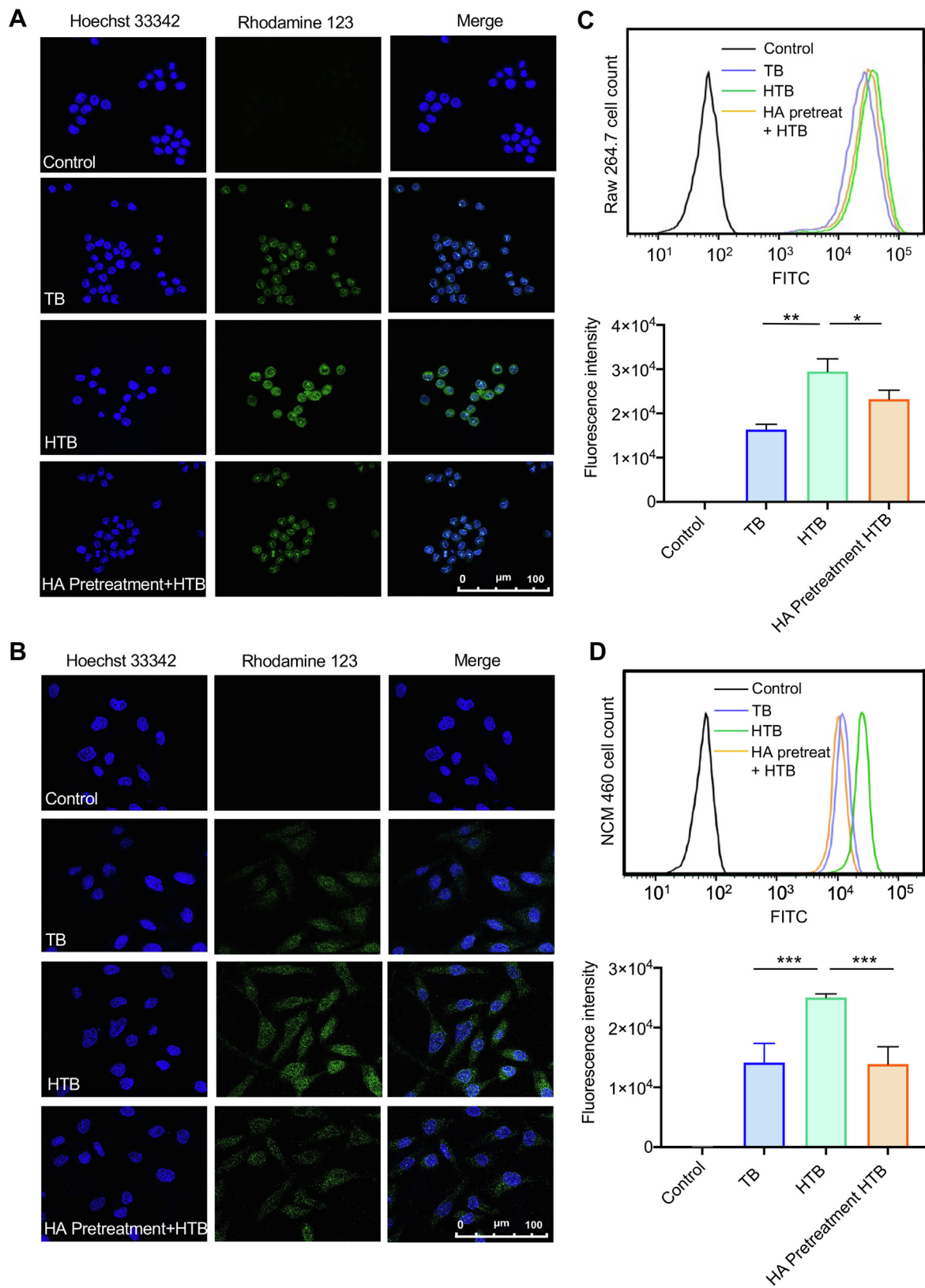


**Fig. 3.** Cellular uptake of TB and HTB. (A) Qualitative analysis and (C) quantitative measurement of TB or HTB in Raw264.7 cells with or without the pretreatment of 1 mg/mL of HA for 4 h. (B) Qualitative analysis and (D) quantitative measurement of TB or HTB in NCM460 cells with or without the pretreatment of HA for 4 h. Data are expressed as mean ± SD (n = 3). \*P < 0.05, \*\*P < 0.01, \*\*\*P < 0.001.

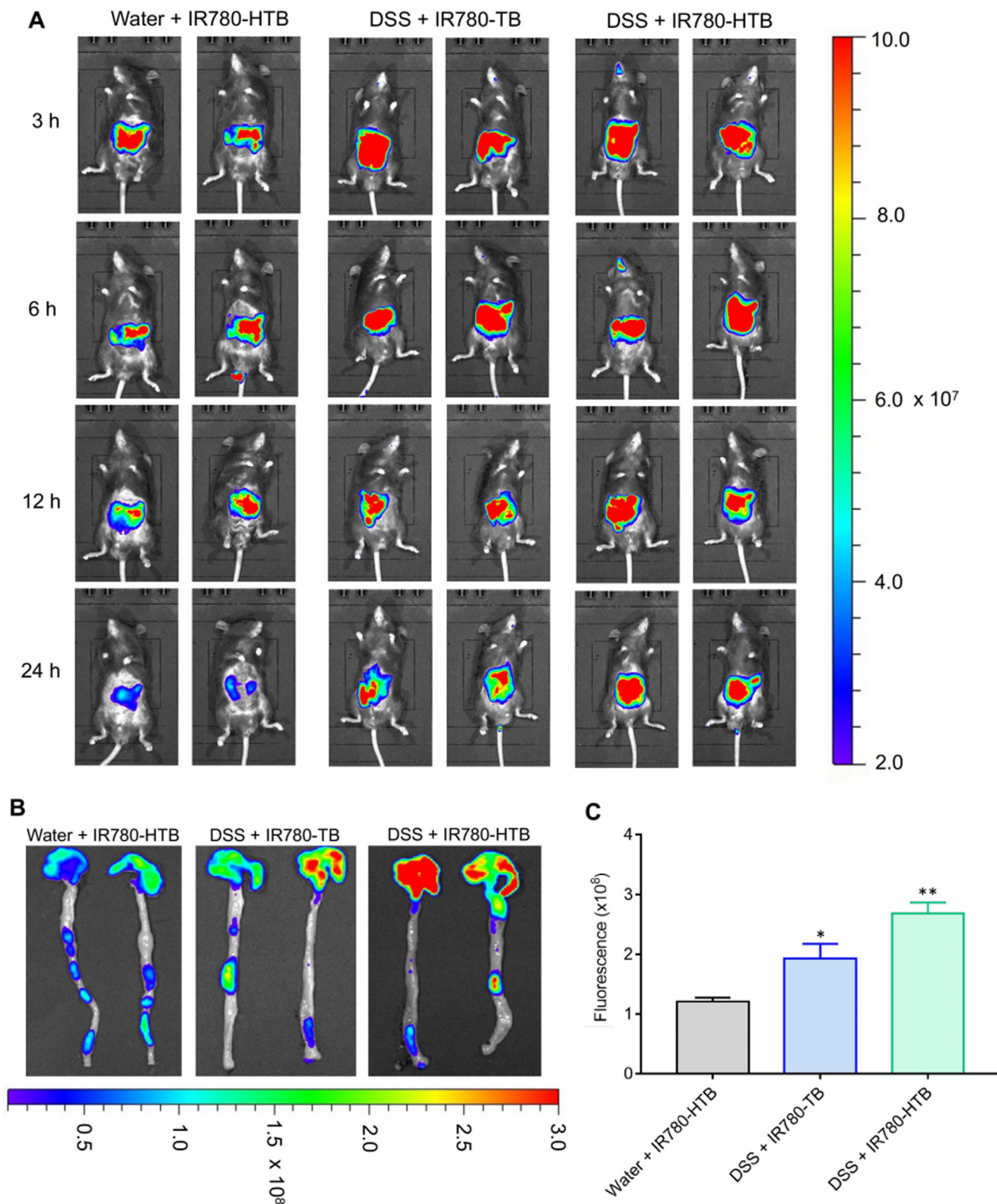


**Fig. 4.** *In vivo* adhesion of TB and HTB. (A) *In vivo* fluorescence imaging of orally delivered IR780-TB and IR780-HTB in colitic and healthy mice. (B) Representative fluorescence images of distal colons separated from colitic and healthy mice after administration for 24 h. (C) Region of interest (ROI) fluorescence intensity of the fluorescence images of distal colons measured with Living Image 4.5 software. Data are expressed as mean ± SD (n = 6). \*P < 0.05 and \*\*P < 0.01.

UC, which could be utilized for targeted drug delivery by using negatively charged vectors. To examine the effect of *in vivo* adherence ability of HTB, DSS-induced UC mice were orally administered with IR780-labelled TB and HTB particles.

As revealed in Fig. 4A, the fluorescence intensity in the healthy intestine of living mice was significantly weaker than that of an inflamed colon at 6, 12, and 24 h. After 12 h, the fluorescence intensity of IR780-labelled HTB in the UC model mice was evidently

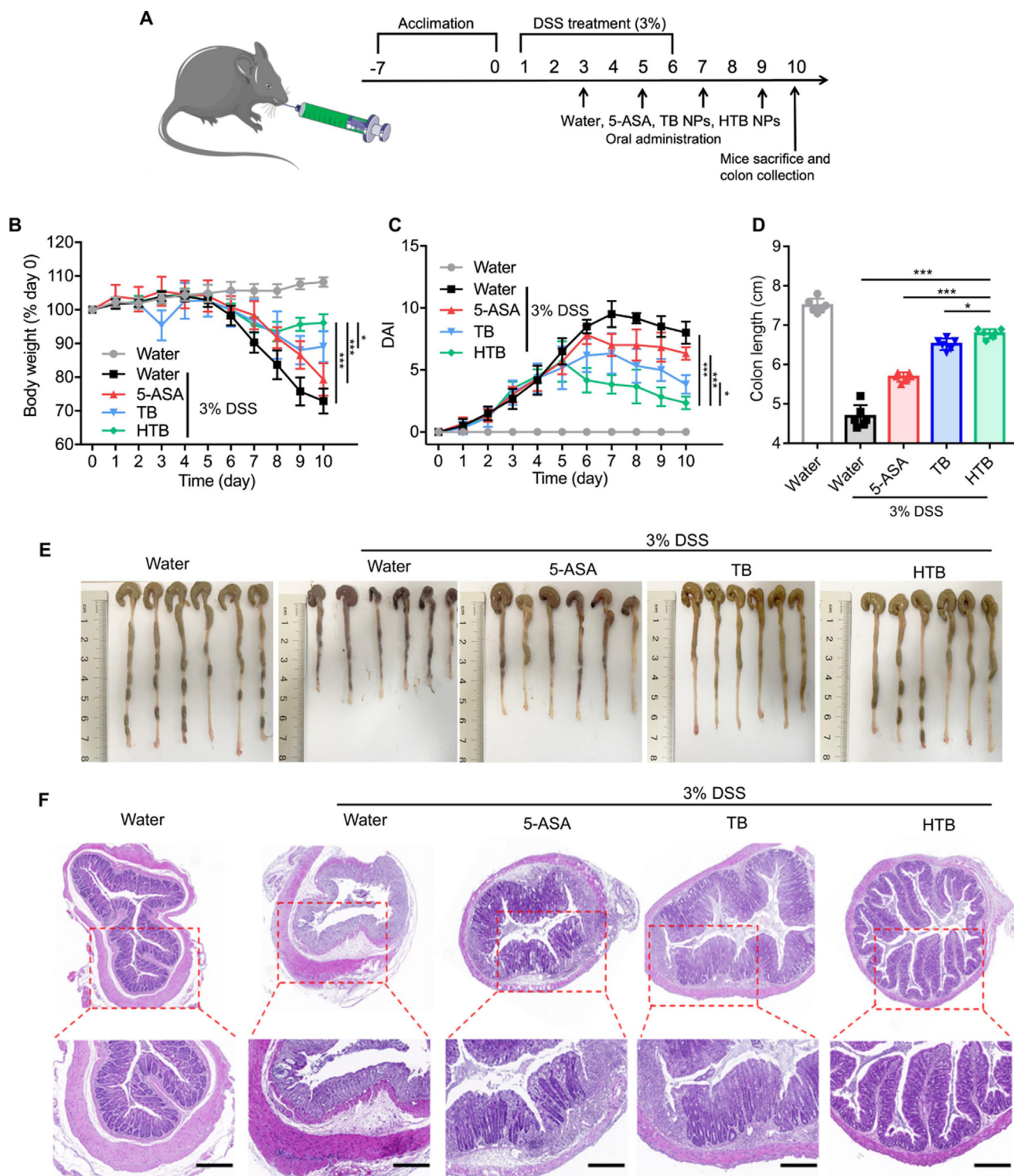


**Fig. 5.** *In vivo* therapeutic effects of HTB. (A) C57BL/6 mice were supplied with water or 3% DSS in drinking water for 11 d. On days 3, 5, 7 and 9, mice were orally administered with TB (BBR at 20 mg/kg), HTB (BBR at 20 mg/kg) or 5-ASA (100 mg/kg). (B) Curve chart changes of mice body weight across time among the five intervention means, normalized to the percentage of the initial body weight. (C) Curve chart variations of *in vivo* DAI scores of mice. (D) Histogram statistics of colon length with different intervention means. (E) Images of mouse colons of different groups. (F) H&E staining of colonic sections after the five different treatments. Scale bar was 200  $\mu$ m. Data are expressed as mean  $\pm$  SD (n = 6). \* $P < 0.05$ , \*\* $P < 0.01$  and \*\*\* $P < 0.001$ .

the strongest, followed by IR780-TB in the UC model mice and IR780-HTB in healthy mice. The difference of fluorescence intensity of IR780 among the three experimental groups was maintained to the 24 h after oral administration. Moreover, the fluorescence

intensity of IR780-labeled HTB in inflamed colons was about 2.5 times higher than that of the healthy colon (Fig. 4B & C). Besides, the average fluorescence strength of IR780-HTB was approximately 1.5 times higher than that of the IR780-TB in inflamed colons.

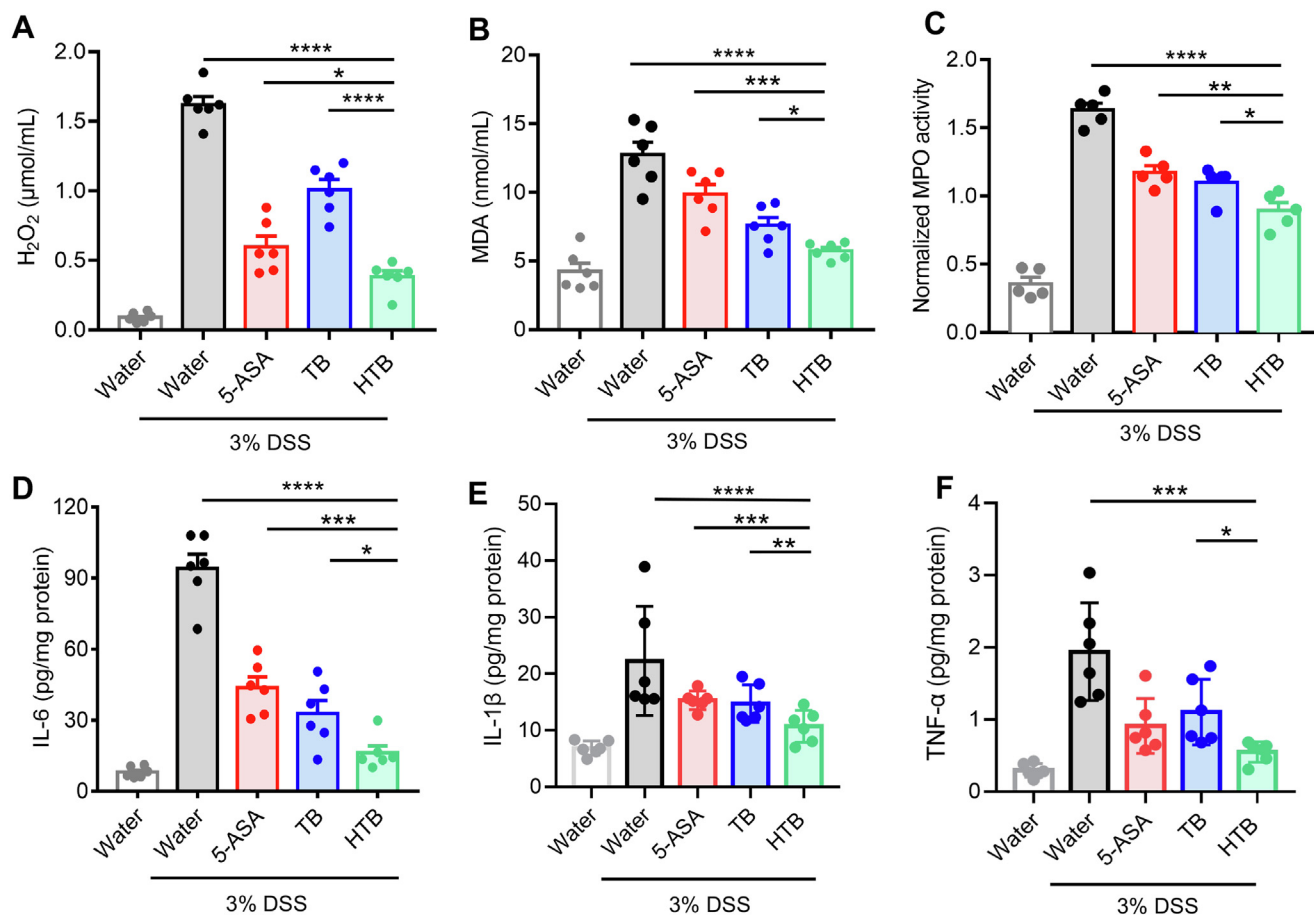


**Fig. 6.** Oxidative stress markers and colonic inflammatory cytokine changes after HTB treatment. (A-B) Histogram analysis of oxidative stress markers (H<sub>2</sub>O<sub>2</sub> and MDA) changes in serum among the five formulations. (C) Histogram analysis of serum MPO expression. (D-F) Histogram analysis of murine colonic inflammatory cytokines (IL-6, IL-1β and TNF-α) changes. Data are presented as mean ± SD (n = 6). \*P < 0.05, \*\*P < 0.01 and \*\*\*P < 0.001.

These results suggested that HTB has an inflamed colon-targetability and the inflamed colon-targeting characteristics of HTB may have great potential in colitis treatment.

#### *In vivo therapeutic efficacy*

The DSS-induced experimental UC mouse model has been demonstrated to resemble clinical UC in the experimental study, which was characterized by colon length reduction, body weight loss, inflammatory cell infiltration and colonic epithelial destruction. Thus, UC mouse model was employed to assess the *in vivo* therapeutic activity of HTB. The intervention schedule is displayed in Fig. 5A. As revealed in Fig. 5B, a 28% decrease of body weight was observed in model group at day 10. Notably, the body weight of the UC mice administered with HTB was only slightly reduced as compared with their initial body weight. Comparatively, the decrease in body weight of the 5-ASA and TB group were higher than that of the mice treated with HTB. Besides, the severity of inflammation was evaluated by using the DAI score, which consists of stool consistency, weight loss and blood in stool. Fig. 5C revealed that DAI of the DSS-induced UC group was obviously improved as compared with the control group from day 5, which demonstrated that the UC model was successfully established. From day 5 to day 10, the DAI score of the HTB group was consistently lower than that of the model, 5-ASA or TB groups. On the last day of the experiment, the DAI score of HTB group mice was  $2.1 \pm 0.38$ , which was proximate to that of the control group and lower than that of the model ( $8 \pm 0.82$ ), 5-ASA ( $6.3 \pm 1.15$ ), and TB ( $4.67 \pm 0.94$ )

groups. In the statistics of colon length, the entire colons in HTB group were evidently longer than that of the model group. In addition, the colon length of the HTB group was longer than that of other treatments (Fig. 5D & E). These results demonstrated that HTB alleviated the typical atrophy of colon induced by DSS.

To further verify the above results, H&E staining of colons was carried out. As revealed in Fig. 5F, DSS led to serious mucosal damages including crypt loss, focal necrosis and influx of inflammatory cells in colonic tissue when compared with the control group. However, mice of the HTB group had more intact crypts and less inflammatory infiltration, indicating that HTB potentially ameliorated the symptoms of colonic inflammation. The above results suggested that HTB could effectively protect against DSS-induced colitis in mice.

#### *HTB regulates colonic inflammatory cytokines*

As shown in the Fig. 6A & B, serum from DSS-induced mice showed notably higher levels of H<sub>2</sub>O<sub>2</sub> and MDA compared to that of the control mice. Oral administration of HTB significantly reduced H<sub>2</sub>O<sub>2</sub> and MDA levels, which were lower than that of the 5-ASA, TB, or model group. We also examined the activity of MPO, an enzyme mainly expressed by activated neutrophils that can be an indicator of the degree of inflammatory status [34]. As shown in Fig. 6C, DSS treatment resulted in a significantly higher level of MPO activity in colon tissue, while HTB group showed the lowest level of MPO activity comparing with 5-ASA or TB-

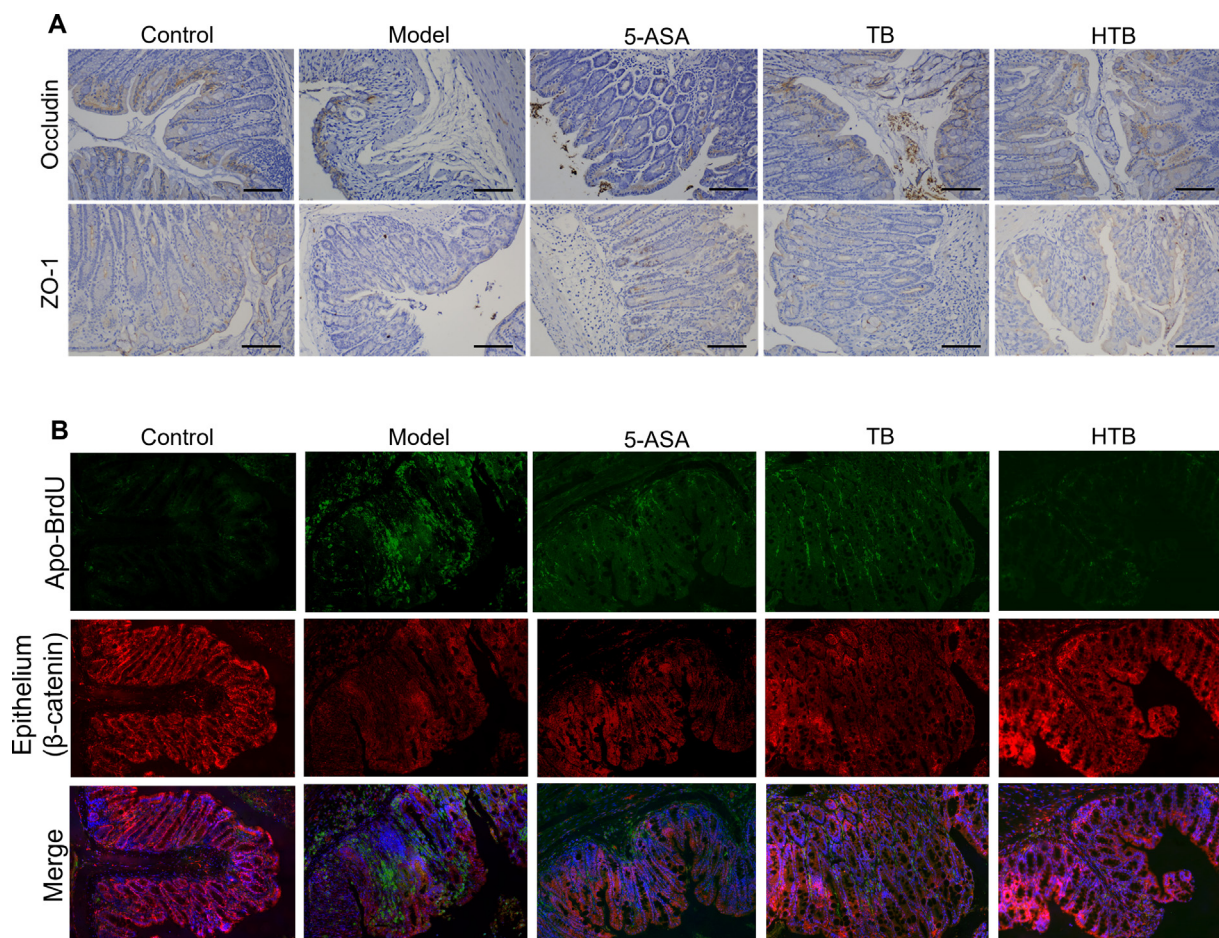


**Fig. 7.** HTB regulates gut barrier function and apoptosis in colitis mice. (A) The expression of ZO-1 protein in colon by IHC assay. Scale bar was 200  $\mu\text{m}$  (B) Colon tissues treated as shown were processed by the immunofluorescence assay, followed by visualization by confocal microscopy. Scale bar was 100  $\mu\text{m}$ . Data are expressed as mean  $\pm$  SD (n = 6).

treated group. Notably, colonic MPO activity in the HTB group was the lowest among all treatment groups.

DSS-induced UC is characterized as increased level of inflammatory mediator and enhanced massive secretion of proinflammatory cytokines, leading to many inflammatory infiltrations and dysfunctions [35]. To assess the anti-inflammatory effect of HTB, the concentration of several pro-inflammatory cytokines was examined by ELISA. As shown in the Fig. 6D-F, the expressions of IL-6, IL-1 $\beta$ , and TNF- $\alpha$  were significantly increased in model group, while treatment of TB or HTB significantly reduced the expression of the pro-inflammatory cytokines. It was noteworthy that the HTB-treated group also had lower levels of these pro-inflammatory cytokines as compared with the TB-treated group, indicating that HTB was more effective in suppressing DSS-induced inflammatory response.

#### HTB regulates gut barrier function and apoptosis

The damage of epithelial barrier function is a typical feature of UC pathophysiology [36]. To examine the effect of TB and HTB on epithelial barrier function in UC, the expression of ZO-1 and occludin, two essential components of the epithelial cytoskeleton, were measured by IHC. As revealed in Fig. 7A, ZO-1 and occludin expression were significantly reduced in colon sections of the DSS-induced group, indicating the epithelial barrier function was significantly damaged after DSS treatment, whereas HTB treatment significantly upregulated their expression in the colon of mice with

DSS-induced colitis. Comparing with the TB and 5-ASA group, the HTB-treated group expressed a higher level of ZO-1 and occludin and had a more intact structure of epithelial barrier. These results indicated that HTB had a better protective effect on the epithelial cytoskeleton. Further, epithelial apoptosis, an important pathogenic initiator of UC, was also examined via immunofluorescence assay. As indicated in Fig. 7B, the ratio of apoptotic epithelial cells was the least in the HTB-treated group, which was indicated by the lowest fluorescence intensity in the HTB treated group, while the 5-ASA or TB treatment could only partially rescue the epithelial cells from cell death. These results indicated that 5-ASA, TB, and HTB protected the epithelial cell survival and the epithelial barrier in the DSS-induced UC model, while HTB had a better protective effect on maintaining the colon tissue architecture.

#### Recovery of gut microbiome by HTB intervention

Annotated OTU data was filtered with a minimum count of 3 and a 10% prevalence cross samples. A total of 494 OTUs were included for further analysis. The results for  $\alpha$  diversity analysis showed that, compared with model group, TB and HTB treatment did not significantly alter indices of Observed species, Shannon and Chao1 (Fig. 8A-C), suggesting unchanged microbial diversity and richness, while the positive drug 5-ASA induced a remarkable decrease of these indices. The PCoA analysis based on the OTU levels demonstrated that the model group was clearly separated out from the control group, suggesting a quite distinct microbial

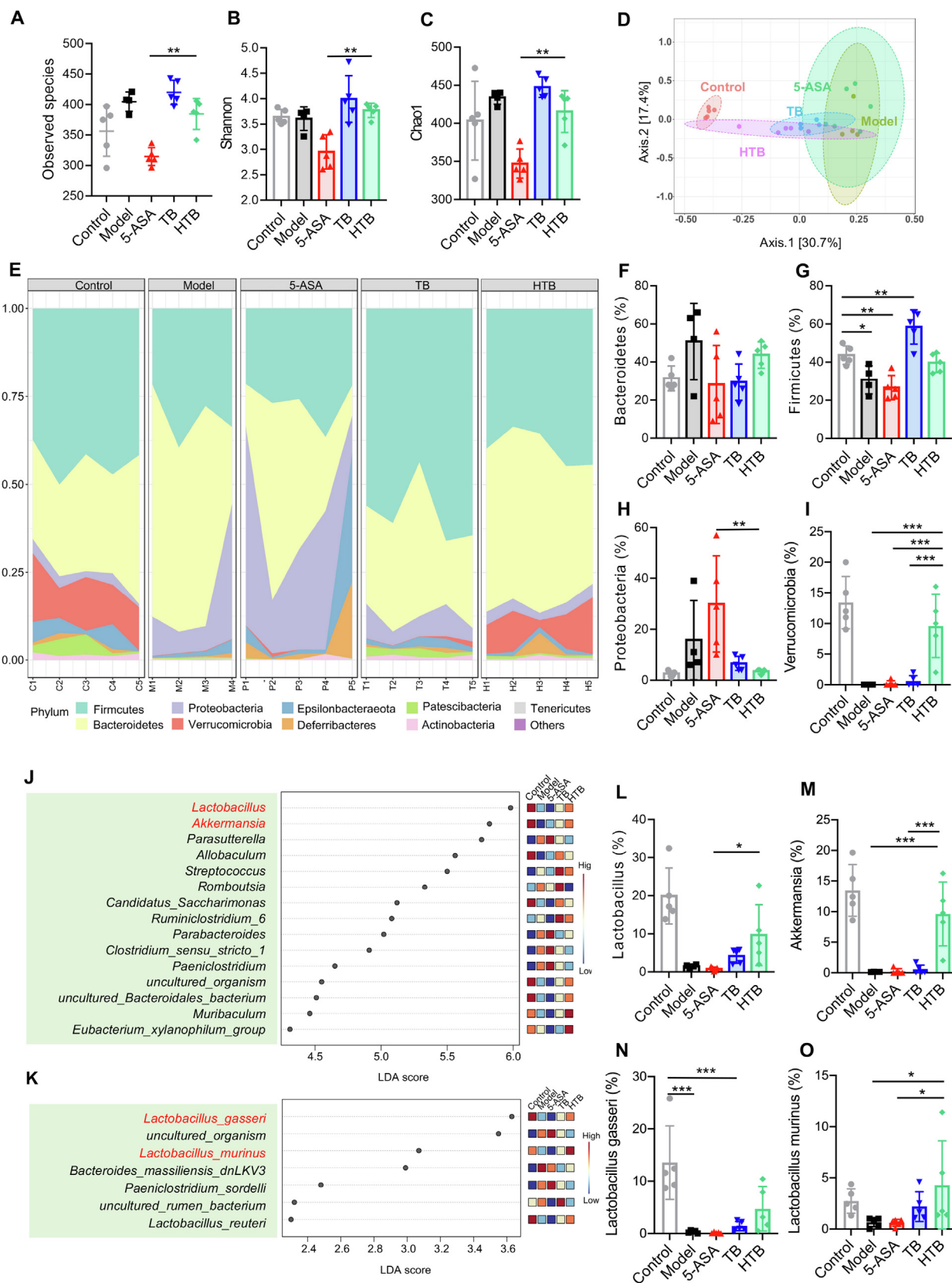


**Fig. 8.** HTB partially recovered DSS-mediated gut microbiome alteration. (A-C) Alpha diversity index of observed species, Shannon and chao1. (D) PcoA analysis at OTU level (displaying top 15 features). (E) Stacked area plot of phylum abundance cross groups. (F-I) Relative abundance of individual phylum. (J) LefSe analysis based on genus level (top 15 features ranked from most significance). (K) LefSe analysis based on species level. (L-M) Genus abundance of *Lactobacillus* and *Akkermansia* bacteria. (N-O) Species abundance of *lactobacillus* bacteria. Data are expressed as mean  $\pm$  SD (n = 4 or 5). \* $P < 0.05$ , \*\* $P < 0.01$  and \*\*\* $P < 0.001$ .

structure. Notably, unlike TB and 5-ASA groups, the HTB group showed a trend moving towards the control group (Fig. 8D). The results indicated that HTB treatment on UC mice at least partially recovered DSS-induced alteration of gut microbial structure.

To clarify how HTB impacted gut microbiome of UC mice, comparison of bacteria at phylum, genus and species levels was further conducted (Table S3–4). The overall pictures of microbial structure based on the abundance of phylum (area plot of 10 most-abundant phyla) and genus (heatmap of 34 most-abundant genus) are displayed in Fig. 8E and Fig. S2, respectively. Although there were remarkable difference among different groups, the microbial structure of control group and HTB group showed the highest similarities. The main identified bacterial phyla were Bacteroidetes, Firmicutes, Proteobacteria and Verrucomicrobia, with their relative abundance shown in Fig. 8F–I. Notably, HTB treatment could recover DSS-mediated gut microbial alterations, including the decrease of Proteobacteria (Fig. 8H) and the increase of Verrucomicrobia (Fig. 8I). Dysbiosis can be characterized as the reduction in microbial diversity and the loss of beneficial bacterias [37]. Proteobacteria has been previously suggested as a potential diagnostic marker for microbial dysbiosis in colitis [38]. Verrucomicrobia includes the *Akkermansia* bacteria that have shown many health benefits [39]. Therefore, HTB is likely to suppress potential pathogenic bacteria and promote beneficial ones.

Furthermore, in order to identify key specific bacterial genus and species associated with different treatment, LEfSe analysis was employed. As displayed in Fig. 8J and Table S5, 15 main genus had high LDA scores (>3), with the beneficial *Lactobacillus* and *Akkermansia* being the most significant ones (Fig. 8L & M). With a closer look, unlike the 5-ASA and TB intervention, HTB treatment significantly increased the DSS-induced reduction of the relative abundance of *Lactobacillus* and *Akkermansia* among other genus. At the species level, *Lactobacillus gasseri* and *Lactobacillus murinus* were identified as the main biomarkers for distinguishing different groups (Fig. 8K and Table S6). Similarly, the relative abundance of *Lactobacillus gasseri* and *Lactobacillus murinus* were significantly decreased in model group, however, the HTB treatment could recover their levels (Fig. 8N & O).

The above results suggested that HTB could mostly recover the DSS-mediated gut microbial alterations at different taxonomy levels. Potentially beneficial bacteria of *Lactobacillus gasseri* and *Lactobacillus murinus* were the key features of HTB intervention on UC mice.

## Conclusion

In this study, a naturally derived and stable drug delivery system was developed for the treatment of UC. Two active ingredients derived from Chinese herb pair, namely TA and BBR, could self-assemble into uniform and stable particles. Coating with HA reversed the surface charge into negative and further increased cellular uptake efficacy and accumulation in inflamed colon lesions. HTB could modulate oxidative stress parameters, inhibit pro-inflammatory cytokines, restore expression of tight junction-associated proteins and recover gut microbiome alteration, thereby exerting strong anti-inflammatory effects against DSS-induced murine acute colitis. We believe our targeted strategy may provide a convenient yet alternative strategy for the treatment of UC and shed light on new modes of application of herbal combinations.

## Compliance with Ethics Requirements

All Institutional and National Guidelines for the care and use of animals were followed.

## CRediT authorship contribution statement

**Shiyun Chen:** Investigation, Writing – original draft. **Zhejie Chen:** Visualization, Writing – original draft. **Yi Wang:** Software, Validation. **Wei Hao:** Investigation, Writing – review & editing. **Qin Yuan:** Investigation. **Hefeng Zhou:** . **Caifang Gao:** Writing – review & editing. **Yitao Wang:** Supervision, Funding acquisition. **Xu Wu:** Conceptualization, Methodology, Supervision. **Shengpeng Wang:** Conceptualization, Methodology, Project administration.

## Declaration of Competing Interest

The authors declare that they have no known competing financial interests or personal relationships that could have appeared to influence the work reported in this paper.

## Acknowledgements

This work was supported by the grants of the Science and Technology Development Fund, Macau SAR (File No. 0151/2020/A3), Guangxi Science and Technology Research Project (GuiKeAA18242040), Guizhou Provincial Administration of Traditional Chinese Medicine Funding (QZYY-2016-062), Major basic and applied basic research projects of Guangdong Province of China (2019B030302005) and the Research Fund of the University of Macau (File No. MYRG2020-00141-ICMS).

## Appendix A. Supplementary material

Supplementary data to this article can be found online at <https://doi.org/10.1016/j.jare.2021.11.017>.

## References

- [1] Danese S, Fiocchi C. Ulcerative Colitis. *N Engl J Med* 2011;365(18):1713–25.
- [2] Ng SC, Tang W, Ching JY, Wong M, Chow CM, Hui AJ, et al. Incidence and phenotype of inflammatory bowel disease based on results from the Asia-Pacific Crohn's and colitis epidemiology study. *Gastroenterology* 2013;145(1):158–165.e152.
- [3] Kaplan GG. The global burden of IBD: from 2015 to 2025. *Nat Rev Gastroenterol Hepatol* 2015;12(12):720–7.
- [4] Guo BJ, Bian ZX, Qiu HC, Wang YT, Wang Y. Biological and clinical implications of herbal medicine and natural products for the treatment of inflammatory bowel disease. *Ann N Y Acad Sci* 2017;1401(1):37–48.
- [5] Gao C, Liu L, Zhou Y, Bian Z, Wang S, Wang Y. Novel drug delivery systems of Chinese medicine for the treatment of inflammatory bowel disease. *Chinese Med* 2019;14(1):23.
- [6] Wang S, Hu Y, Tan W, Wu X, Chen R, Cao J, et al. Compatibility art of traditional Chinese medicine: from the perspective of herb pairs. *J Ethnopharmacol* 2012;143(2):412–23.
- [7] Chen Z, Farag MA, Zhong Z, Zhang C, Yang Y, Wang S, et al. Multifaceted role of phyto-derived polyphenols in nanodrug delivery systems. *Adv Drug Deliv Rev* 2021;176:113870.
- [8] Wang J, Wang L, Lou G-H, Zeng H-R, Hu J, Huang Q-W, et al. *Coptidis Rhizoma*: a comprehensive review of its traditional uses, botany, phytochemistry, pharmacology and toxicology. *Pharm Biol* 2019;57(1):193–225.
- [9] Meng F-C, Wu Z-F, Yin Z-Q, Lin L-G, Wang R, Zhang Q-W. *Coptidis rhizoma* and its main bioactive components: recent advances in chemical investigation, quality evaluation and pharmacological activity. *Chinese Med* 2018;13(1):13.
- [10] Zhao T, Tang H, Xie L, Zheng Y, Ma Z, Sun Q, et al. *Scutellaria baicalensis* Georgi. (Lamiaceae): a review of its traditional uses, botany, phytochemistry, pharmacology and toxicology. *J Pharm Pharmacol* 2019;71(9):1353–69.
- [11] Li T, Wang P, Guo W, Huang X, Tian X, Wu G, et al. Natural Berberine-Based Chinese Herb Medicine Assembled Nanostructures with Modified Antibacterial Application. *ACS Nano* 2019;13(6):6770–81.
- [12] Huang X, Wang P, Li T, Tian X, Guo W, Xu B, et al. Self-Assemblies Based on Traditional Medicine Berberine and Cinnamic Acid for Adhesion-Induced Inhibition Multidrug-Resistant *Staphylococcus aureus*. *ACS Appl Mater Interfaces* 2020;12(1):227–37.
- [13] Zheng Q-x, Wu H-f, Guo J, Nan H-j, Chen S-l, Yang J-s et al.: Review of *Rhubarbs*: Chemistry and Pharmacology. *Chinese Herbal Med* 2013;5(1):9–32.
- [14] Deng W-W, Zong Y, Xiao Y-X. Hexafluoroisopropanol-Based Deep Eutectic Solvent/Salt Aqueous Two-Phase Systems for Extraction of Anthraquinones from *Rhei Radix* et *Rhizoma* Samples. *ACS Sustainable Chem Eng* 2017;5(5):4267–75.

- [15] Xu L, Zhang Y, Xue X, Liu J, Li ZS, Yang GY, et al. A Phase I Trial of Berberine in Chinese with Ulcerative Colitis. *Cancer Prevent Res (Philadelphia, Pa)* 2020;13(1):117–26.
- [16] Yang Y, Vong CT, Zeng S, Gao C, Chen Z, Fu C, et al. Tracking evidences of *Coptis chinensis* for the treatment of inflammatory bowel disease from pharmacological, pharmacokinetic to clinical studies. *J Ethnopharmacol* 2021;268:113573.
- [17] Xiao HT, Wen B, Shen XC, Bian ZX. Potential of Plant-sourced Phenols for Inflammatory Bowel Disease. *Curr Med Chem* 2018;25(38):5191–217.
- [18] Wittig BM, Johansson B, Zöller M, Schwärzler C, Günther U. Abrogation of experimental colitis correlates with increased apoptosis in mice deficient for CD44 variant exon 7 (CD44v7). *J Exp Med* 2000;191(12):2053–64.
- [19] Zhou Y, Liu S-q, Peng H, Yu L, He B, Zhao Q. In vivo anti-apoptosis activity of novel berberine-loaded chitosan nanoparticles effectively ameliorates osteoarthritis. *Int Immunopharmacol* 2015;28(1):34–43.
- [20] Patel AR, Seijen-ten-Hoorn J, Heussen PCM, Drost E, Hazekamp J, Velikov KP. Straightforward preparation of organic colloidal particles by harnessing spontaneous non-covalent interactions of active molecules from natural origin. *J Colloid Interface Sci* 2012;374(1):150–6.
- [21] Luo R, Lin M, Zhang C, Shi J, Zhang S, Chen Q, et al. Genipin-crosslinked human serum albumin coating using a tannic acid layer for enhanced oral administration of curcumin in the treatment of ulcerative colitis. *Food Chem* 2020;330:127241.
- [22] Wang Y, Tao H, Huang H, Xiao Y, Wu X, Li M, et al. The dietary supplement *Rhodiola crenulata* extract alleviates dextran sulfate sodium-induced colitis in mice through anti-inflammation, mediating gut barrier integrity and reshaping the gut microbiome. *Food Funct* 2021;12(7):3142–58.
- [23] Gupta RA, Motiwala MN, Dumore NG, Danao KR, Ganjare AB. Effect of piperine on inhibition of FFA induced TLR4 mediated inflammation and amelioration of acetic acid induced ulcerative colitis in mice. *J Ethnopharmacol* 2015;164:239–46.
- [24] Magoč T, Salzberg SL. FLASH: fast length adjustment of short reads to improve genome assemblies. *Bioinformatics* 2011;27(21):2957–63.
- [25] Chong J, Liu P, Zhou G, Xia J. Using MicrobiomeAnalyst for comprehensive statistical, functional, and meta-analysis of microbiome data. *Nat Protoc* 2020;15(3):799–821.
- [26] Kim H-Y. Analysis of variance (ANOVA) comparing means of more than two groups. *Restorative Dentistry Endodontics* 2014;39(1):74–7.
- [27] Boonsongrit Y, Mueller BW, Mitrevej A. Characterization of drug–chitosan interaction by <sup>1</sup>H NMR, FTIR and isothermal titration calorimetry. *Eur J Pharm Biopharm* 2008;69(1):388–95.
- [28] Muhoza B, Xia S, Zhang X. Gelatin and high methyl pectin coacervates crosslinked with tannic acid: The characterization, rheological properties, and application for peppermint oil microencapsulation. *Food Hydrocolloids* 2019;97:105174.
- [29] Wu S-J, Don T-M, Lin C-W, Mi F-L. Delivery of Berberine Using Chitosan/Fucoidan-Taurine Conjugate Nanoparticles for Treatment of Defective Intestinal Epithelial Tight Junction Barrier. *Mar Drugs* 2014;12(11).
- [30] Lee SH, Bajracharya R, Min JY, Han J-W, Park BJ, Han H-K. Strategic Approaches for Colon Targeted Drug Delivery: An Overview of Recent Advancements. *Pharmaceutics* 2020;12(1).
- [31] Tirosh B, Khatib N, Barenholz Y, Nissan A, Rubinstein A. Transferrin as a Luminal Target for Negatively Charged Liposomes in the Inflamed Colonic Mucosa. *Mol Pharm* 2009;6(4):1083–91.
- [32] Monajemi H, Meenan J, Lamping R, Obradov DO, Radema SA, Trown PW, et al. Inflammatory bowel disease is associated with increased mucosal levels of bactericidal/permeability-increasing protein. *Gastroenterology* 1996;110(3):733–9.
- [33] Ho S, Pothoulakis C, Koon HW. Antimicrobial peptides and colitis. *Current Pharmc Des* 2013;19(1):40–7.
- [34] Das P, Goswami P, Das TK, Nag T, Sreenivas V, Ahuja V, et al. Comparative tight junction protein expressions in colonic Crohn's disease, ulcerative colitis, and tuberculosis: a new perspective. *Virchows Archiv: Int J Pathol* 2012;460(3):261–70.
- [35] Perše M, Cerar A. Dextran Sodium Sulphate Colitis Mouse Model: Traps and Tricks. *J Biomed Biotechnol* 2012;2012:718617.
- [36] Gitter AH, Wullstein F, Fromm M, Schulzke JD. Epithelial barrier defects in ulcerative colitis: Characterization and quantification by electrophysiological imaging. *Gastroenterology* 2001;121(6):1320–8.
- [37] Carding S, Verbeke K, Vipond DT, Corfe BM, Owen LJ. Dysbiosis of the gut microbiota in disease. *Microbial Ecol Health Disease* 2015;26(1):26191.
- [38] Shin NR, Whon TW, Bae JW. Proteobacteria: microbial signature of dysbiosis in gut microbiota. *Trends Biotechnol* 2015;33(9):496–503.
- [39] Ou Z, Deng L, Lu Z, Wu F, Liu W, Huang D, et al. Protective effects of *Akkermansia muciniphila* on cognitive deficits and amyloid pathology in a mouse model of Alzheimer's disease. *Nutr Diabetes* 2020;10(1):12.